Why Potential Vorticity Is Not Conserved along Mean Streamlines in a Numerical Southern Ocean

SARAH T. GILLE

Physical Oceanography Research Division, Scripps Institution of Oceanography, La Jolla, California

(Manuscript received 16 July 1996, in final form 2 December 1996)

ABSTRACT

Potential vorticity (PV) is used as an indicator of the forcing processes and dissipation at work in the Southern Ocean. Output from the Semtner–Chervin model run with quarter-degree resolution is considered on isopycnal surfaces along Montgomery streamfunctions. Numerical results are compared with hydrographic measurements. Although simple hypotheses might suggest that subsurface PV should be unaffected by wind forcing and constant along streamlines, these results indicate that even at about 1000-m depth, PV varies along mean streamlines in both the numerical model output and in the in situ observations. The changes in PV are largely represented by stratification changes rather than shifts in the Coriolis parameter or in relative vorticity. In the numerical model output, a combination of mechanisms is responsible for these changes in PV, including transient tracer fluxes, transient momentum fluxes, diffusive processes, and long-term tracer drift.

1. Introduction

Potential vorticity has been extensively considered as a tracer for ocean circulation. Easily derived from the vorticity and tracer conservation equations, potential vorticity (PV) behaves differently than a passive tracer. It has two features that make it particularly attractive for analyzing ocean circulation. First, if relative vorticity is small, then PV may be computed directly from the vertical density structure, as measured in hydrographic surveys. Second, in an unforced and nondissipative system, PV is conserved along geostrophic streamlines (see Pedlosky 1987). Thus, if flow is along geostrophic streamlines (as the quasigeostrophic approximation would dictate) and either the isopycnal surface is deep enough so that no direct forcing acts or else forcing is dissipated in the same geographic locations where it acts, then PV will be constant along streamlines. Under different circumstances, if streamlines are closed and a small amount of dissipation is present, then PV may be diffused along isopycnal surfaces in which case it should be constant, not only on streamlines but over the entire isopycnal surface (Rhines and Young 1982). Alternatively, if forcing is substantial or if dissipation is more than just a uniform effect due to the background eddy field, then PV will undergo dramatic changes in value along streamlines; the geographic locations of these changes may be useful indicators of the leading mechanisms controlling the dynamics.

Several recent studies have taken advantage of PV to probe Southern Ocean dynamics. Marshall et al. (1993) used the concept of PV homogenization outlined by Rhines and Young (1982) as a starting point. They noted that, if nothing forces a layer of the ocean, as they suggested might be expected below the wind-forced surface layer of the Antarctic Circumpolar Current (ACC), then as flow loops around closed streamlines, background eddy processes should homogenize PV on isopycnal surfaces. Based on hydrographic data, they suggested that PV varies linearly with potential density. Employing this linear functional relationship and hydrographic measurements at one depth only, they predicted dynamic topography in the Atlantic sector of the ACC. Discrepancies between their results and more detailed hydrography, they suggested, indicated locations where the uniform PV assumption was less satisfactory.

Marshall (1995) further explored the implications of determining PV as a function of potential density. By also requiring that PV be conserved along streamlines, that density be constant along streamlines on the sea floor, and that the linear vorticity balance apply, he derived an analytic expression for streamlines. Using realistic bathymetry, but applying no surface wind stress curl, he predicted the path of the ACC to be substantially steered by topography.

This investigation will take an alternative tack. Rather than assuming PV is conserved on isopycnal streamlines or homogenized over isopycnal surfaces, this study will examine the variation of PV along streamlines in order to probe the forcing and dissipation of the ACC.

Corresponding author address: Dr. Sarah T. Gille, Physical Oceanography Research Division, Scripps Institution of Oceanography, La Jolla, CA 92093-0230.
E-mail: sgille@ucsd.edu

Potential vorticity is considered along potential density surfaces in numerical model output in section 2. Since PV turns out to be neither homogenized nor conserved along streamlines, section 2c examines the specific mechanisms responsible for its fluctuations in the numerical model. In section 3 hydrographic data will be examined to show how observations resemble and differ from the numerical model output. Finally, the results are summarized in section 4.

2. Potential vorticity on isopycnals in numerical model output

a. Defining potential vorticity

The Semtner–Chervin model is a global general circulation model based on the Cox–Bryan primitive equation code (Semtner 1986). Although the specifics of the resolution and forcing differ, the basic model is the same as the Fine Resolution Antarctic Model (FRAM) (FRAM Group 1991), and the resulting momentum balances are qualitatively similar (Ivchenko et al. 1996; Stevens and Ivchenko 1997; Gille 1997). Wells and de Cuevas (1995) looked at the vorticity balance along vertically integrated streamlines in the FRAM output, concluding that surface wind stress is balanced by bottom pressure torque localized at Drake Passage; Killworth and Nanneh (1994) considered the momentum balance in isopycnal coordinates to examine how surface wind stress is transferred through the water column as interfacial form drag; however, neither study merged the two to consider potential vorticity on isopycnal surfaces.

For this study, results were analyzed from the ''quarter-degree'' version of the Semtner–Chervin Parallel Ocean Climate Model, which implemented several refinements from the earlier half-degree version (Semtner and Chervin 1992). The horizontal resolution is 0.4° in the zonal direction and 0.4° cos(ϕ) in the meridional direction, which is marginally eddy-resolving. In addition, a free sea surface was included based on the formulation by Killworth et al. (1991). The model was initialized with the output from the half-degree model following 22.5 years of spinup and 10 years of forcing with Hellerman and Rosenstein (1983) winds. During the last 5 years of the half-degree run, all deep relaxation to the Levitus (1982) climatology was eliminated (Semtner and Chervin 1992; A. Semtner 1994, personal communication). At one-quarter degree resolution, the model was then run for one year using climatological winds. Finally, it was forced with ECMWF operational forecast model winds (Trenberth et al. 1989) for the period from January 1986 to December 1989. Surface buoyancy forcing was based on the Levitus monthly climatologies with a one-month relaxation timescale. In addition, temperature and salinity were relaxed to ''annual mean Levitus'' climatology in the upper 2000 m, within 7° of the northern and southern boundaries of the model domain and within 7° of the Strait of Gibraltar using a three-month timescale. Unlike older implementations of the model, this version included no relaxation to the Levitus climatology below 2000 m. The final 3.75 years of the model run, starting with April 1986, were continuously time-averaged to produce statistics, including the means, variances, and covariances of all model variables.

Although the model was run using 20 isobaric levels in the vertical, the results are easily interpolated onto surfaces of constant potential density. The model's horizontal equation of motion on an isopycnal surface may be written:

$$\frac{\partial \mathbf{u}}{\partial t} + f\mathbf{k} \times \mathbf{u} + (\mathbf{u}\cdot\boldsymbol{\nabla})\mathbf{u} + w\frac{\partial \mathbf{u}}{\partial z} + \boldsymbol{\nabla} M = \mu\frac{\partial^2 \mathbf{u}}{\partial z^2} + A_m\nabla^4\mathbf{u}, \quad (1)$$

(e.g., Andrews et al. 1987) where $\mathbf{u}$ is the horizontal velocity vector, w is the vertical velocity, f is the Coriolis parameter, μ is a vertical viscosity coefficient, A_m is the horizontal viscosity coefficient, and $\boldsymbol{\nabla}$ is the two-dimensional horizontal gradient operator. Here M is the Montgomery streamfunction that represents the pressure term transformed into isopycnal coordinates, while ($\mathbf{k} \times \boldsymbol{\nabla} M$)/$f$ represents the horizontal geostrophic velocity on the isopycnal surface.

The streamfunction M should be carefully defined. Although McDougall (1989) pointed out that no correct streamfunction exists for potential density surfaces, Zhang and Hogg (1992) showed that the geostrophic streamlines on potential density surfaces may be approximated by the Montgomery streamfunction on a surface of constant specific volume anomaly δ, so that

$$M = \delta(z)(p(z) - \bar{p}) - \int^{p} \delta(z)\, dp, \quad (2)$$

where z represents the depth of the isopycnal surface and varies spatially, and

$$\delta(z) = \frac{1}{\rho(z)} - \frac{1}{\rho_0(z)}, \quad (3)$$

where $\rho(z)$ is the in situ density and $\rho_o(z)$ is the density of a reference fluid parcel, here defined with salinity 34.6 psu and temperature 2.33°C to match mean values along the ACC core on the isopycnal $\sigma_1 = 32.3$. The $\sigma_1 = 32.3$ surface has been selected for the results shown in this paper, because it is below the mixed layer and above the ocean floor through most of the Southern Ocean, and it is about 1000 m deep in the core of the ACC. Other middepth isopycnals indicate qualitatively similar trends and will not be shown here. The mean pressure at 1000-m depth, $\bar{p}$, is subtracted in order to minimize errors associated with the approximation.

The addition of a free surface η means that M may be written:

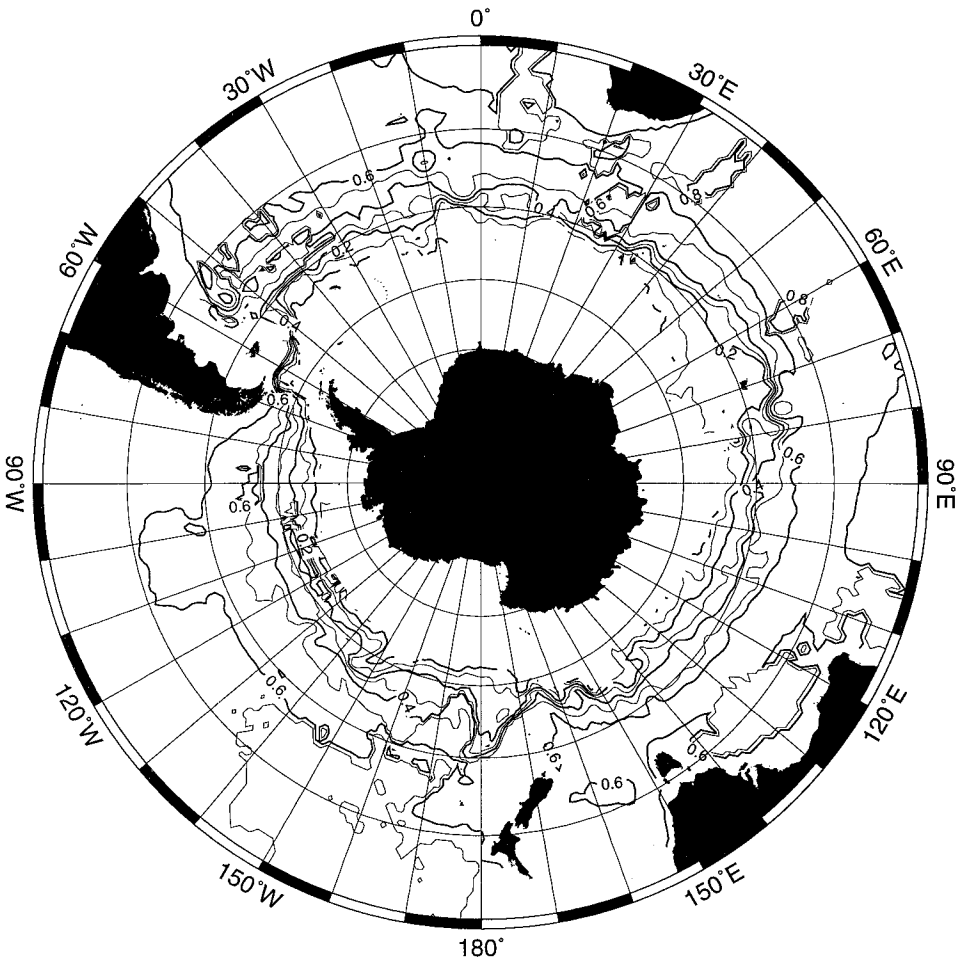

FIG. 1. Contours of constant Montgomery streamfunction divided by $g\rho_o$ (in m) on the potential density surface $\sigma_1 = 32.3$, determined from the Semtner–Chervin quarter-degree numerical model. The contour interval is 0.1 m, and the 0-m height contour is fixed arbitrarily. Data are not shown where $\sigma_1 = 32.3$ rises above 500-m depth.

$$M = \delta\eta g\rho_s + \delta\int_z^0 g\rho\, dz' - \delta\overline{p} - \int^p \delta\, dp. \quad (4)$$

Here M for the Semtner–Chervin model output at $\sigma_1 = 32.3$ is contoured in Fig. 1. The streamfunction M closely resembles sea surface height, η, represented in Fig. 2: both M and η show a similar zonal flow structure, and both figures indicate that the flow intensifies like a western boundary current just downstream of major topographic features at Drake Passage, Campbell Plateau, and Kerguelen Island. The smaller overall height difference for M compared with the sea surface height illustrates the degree to which velocities along the potential density surface are attenuated relative to the ocean's surface.

Time-averaging the momentum equation (1) and then taking the curl produces the vorticity equation:

$$\frac{\zeta_f - \zeta_i}{\Delta t} + \frac{1}{f}J(\overline{M}, \overline{\zeta} + f) + \overline{w}\frac{\partial\overline{\zeta}}{\partial z} + \overline{\mathbf{u}}_{ag}\cdot\nabla(\overline{\zeta} + f) + \nabla\cdot(\overline{\mathbf{u}'\zeta'}) + \overline{w'\frac{\partial\zeta'}{\partial z}}$$
$$= (f + \overline{\zeta})\frac{\partial\overline{w}}{\partial z} + \mu\frac{\partial^2\overline{\zeta}}{\partial z^2} + A_m\nabla^4\overline{\zeta} - \left(\overline{\frac{\partial w}{\partial x}\frac{\partial v}{\partial z}} - \overline{\frac{\partial w}{\partial y}\frac{\partial u}{\partial z}}\right), \quad (5)$$

where overbars represent time averages, and primes represent deviations from those averages, so that $\overline{\mathbf{u}'} = 0$; J is the Jacobian operator, ζ is the relative vorticity ($\partial v/\partial x - \partial u/\partial y$), Δt is 3.75 yr corresponding to the duration of the archived model run, ζ_i and ζ_f are initial and final values of the relative vorticity from the beginning and end of the time interval analyzed, and $\bar{\mathbf{u}}_{ag}$ is the mean ageostrophic horizontal velocity equal to $\bar{\mathbf{u}} - (\mathbf{k} \times \nabla \bar{M})/f$. The transient horizontal velocity $\mathbf{u}'$ is not separated into geostrophic and ageostrophic components. The term $\overline{(\partial w/\partial x)(\partial v/\partial z)} - \overline{(\partial w/\partial y)(\partial u/\partial z)}$ and the vertical viscosity term $\mu\partial^2\zeta/\partial z^2$ are negligibly small and will be omitted in the remainder of this discussion.

The model tracer conservation equation on a level is

$$\frac{\partial \sigma}{\partial t} + (\mathbf{u}\cdot\nabla)\sigma + w\frac{\partial \sigma}{\partial z} = A_H\nabla^4\sigma + F(\sigma), \qquad (6)$$

where σ is a tracer and may represent temperature, salinity, or some combination of the two. For this analysis, σ will be the combination of temperature and salinity corresponding to potential density referenced to 1000-m depth; A_H is the horizontal diffusion coefficient. The function $F(\sigma)$ represents convective adjustment, which is not recorded in the model output but is estimated to be neglible at middepth. Model convective adjustment may be weaker than real ocean conditions would dictate since there is no sea ice model and the Levitus seasonal climatology includes only limited wintertime observations. It will not be included in this analysis, and any residual convective effects will appear in the transient tracer advection terms.

The tracer equation (6) is time-averaged, rewritten as an expression for w, and vertically differentiated to produce

$$\begin{aligned}\frac{\partial \bar{w}}{\partial z} = {} & \frac{\partial}{\partial z}\left[-\frac{\sigma_f - \sigma_i}{\Delta t}\left(\frac{\partial \bar{\sigma}}{\partial z}\right)^{-1}\right] - \left(\frac{\partial \bar{\mathbf{u}}}{\partial z}\cdot\nabla\right)\bar{\sigma}\left(\frac{\partial \bar{\sigma}}{\partial z}\right)^{-1} \\ & - (\bar{\mathbf{u}}\cdot\nabla)\frac{\partial \bar{\sigma}}{\partial z}\left(\frac{\partial \bar{\sigma}}{\partial z}\right)^{-1} + (\bar{\mathbf{u}}\cdot\nabla)\bar{\sigma}\frac{\partial^2 \bar{\sigma}}{\partial z^2}\left(\frac{\partial \bar{\sigma}}{\partial z}\right)^{-2} \\ & + \frac{\partial}{\partial z}\left[A_h\nabla^4\bar{\sigma}\left(\frac{\partial \bar{\sigma}}{\partial z}\right)^{-1} - \overline{w'\frac{\partial \sigma'}{\partial z}}\left(\frac{\partial \bar{\sigma}}{\partial z}\right)^{-1}\right. \\ & \left. - \overline{(\mathbf{u}'\cdot\nabla)\sigma'}\left(\frac{\partial \bar{\sigma}}{\partial z}\right)^{-1}\right]. \qquad (7)\end{aligned}$$

The expression $(\mathbf{u}\cdot\nabla)\sigma(\partial\sigma/\partial z)^{-1} = u\partial h/\partial x + v\partial h/\partial y$ represents the vertical velocity along an isopycnal of height h, due to the tilting of the surface. The difference between the isopycnic vertical velocity and the total vertical velocity w is the diapycnal velocity e. Thus,

$$e = w - (\mathbf{u}\cdot\nabla)\sigma\left(\frac{\partial \sigma}{\partial z}\right)^{-1}. \qquad (8)$$

Since the Semtner–Chervin code is conceived on levels rather than isopycnal layers, tracers are not specifically conserved on layers and the cross-isopycnal velocity e is nonzero but small.

Projecting the tracer evolution equation (7) onto an isopycnal surface will not alter any of the terms in the local balance. Thus, (7) can be substituted directly into the vorticity equation (5) to produce an expression for evolution of PV on isopycnals:

$$\begin{aligned}\frac{1}{f}J(\bar{M}, \bar{Q}) + {} & (\bar{\mathbf{u}}\cdot\nabla)\bar{\sigma}\frac{\partial \bar{Q}}{\partial z}\left(\frac{\partial \bar{\sigma}}{\partial z}\right)^{-1} + \bar{\mathbf{u}}_{ag}\cdot\nabla\bar{Q} + \bar{e}\frac{\partial \bar{\zeta}}{\partial z}\frac{\partial \bar{\sigma}}{\partial z} \\ = {} & -\frac{\zeta_f - \zeta_i}{\Delta t}\frac{\partial \bar{\sigma}}{\partial z} - \bar{Q}\frac{\partial}{\partial z}\left[\frac{\sigma_f - \sigma_i}{\Delta t}\left(\frac{\partial \bar{\sigma}}{\partial z}\right)^{-1}\right] \\ & - \left(\nabla\cdot\overline{(\mathbf{u}'\zeta')} + \overline{w'\frac{\partial \zeta'}{\partial z}}\right)\frac{\partial \bar{\sigma}}{\partial z} - \overline{Q(\mathbf{u}'\cdot\nabla)\sigma'}\left(\frac{\partial \bar{\sigma}}{\partial z}\right)^{-1} \\ & - \bar{Q}\overline{w'\frac{\partial \sigma'}{\partial z}}\left(\frac{\partial \bar{\sigma}}{\partial z}\right)^{-1} - (f + \bar{\zeta})\left(\frac{\partial \bar{\mathbf{u}}}{\partial z}\cdot\nabla\right)\bar{\sigma} \\ & + A_m\nabla^4\bar{\zeta}\frac{\partial \bar{\sigma}}{\partial z} + \bar{Q}\frac{\partial}{\partial z}\left[A_h\nabla^4\bar{\sigma}\left(\frac{\partial \bar{\sigma}}{\partial z}\right)^{-1}\right]. \qquad (9)\end{aligned}$$

Potential vorticity Q is defined in the conventional form

$$Q = (f + \zeta)\left(\frac{\partial \sigma}{\partial z}\right). \qquad (10)$$

Müller (1995) provides a thorough review of the scaling arguments used to derive standard expressions for Q. Equation (9) shows that $D\bar{Q}/dt$ (the terms on the left and the first two terms on the right) is balanced by dissipation in the form of eddy fluxes, viscosity, and diffusion. It differs from more familiar PV equations only because all of the terms representing vertical advection, transient advection, time dependence, horizontal diffusion, and viscosity have been retained.

Each of the terms in (9) accounts for different physical processes in the PV balance: $J(M, Q)$ indicates the change in mean PV along a mean geostrophic streamline $\bar{M}$ due to horizontal advection, while $(\bar{\mathbf{u}}\cdot\nabla)\bar{\sigma}\partial\bar{Q}/\partial z(\partial\bar{\sigma}/\partial z)^{-1}$ accounts for the vertical advection of PV along streamlines. The sum of these first two terms projected along a streamline indicates how advection changes PV along a depth-varying geostrophic streamline. The third term in (9), $\bar{\mathbf{u}}_{ag}\cdot\nabla\bar{Q}$, represents changes in PV due to ageostrophic horizontal velocities, and the fourth term, $\bar{e}\partial\bar{\zeta}/\partial z\partial\bar{\sigma}/\partial z$, is vertical advection across isopycnal surfaces due to the diapycnic vertical velocity e. Both the ageostrophic and diapycnal terms are negligible at middepth and will be omitted in the remainder of this analysis.

The advection of mean PV on the left side of (9) is balanced by a combination of tendency, transient eddy flux, and diffusive terms. The change in PV due to relative vorticity evolution over the model's duration Δt is represented by $(\zeta_f - \zeta_i)/\Delta t\partial\bar{\sigma}/\partial z$, while the corresponding change due to tracer drift is

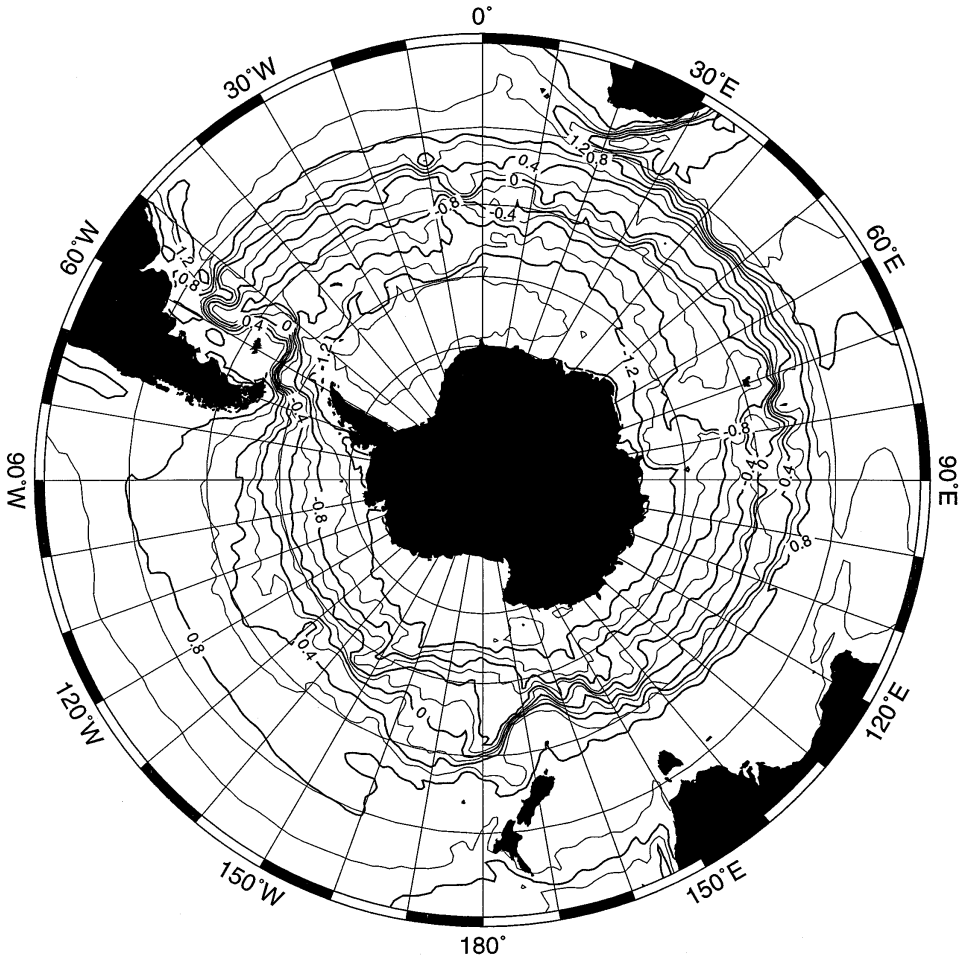

FIG. 2. Contours of sea surface height (in m) from the Semtner–Chervin quarter-degree numerical model. The contour interval is 0.2 m, and the 0-m contour is fixed arbitarily.

$$\bar{Q}\frac{\partial}{\partial z}\left[\frac{\sigma_f - \sigma_i}{\Delta t}\left(\frac{\partial\bar{\sigma}}{\partial z}\right)^{-1}\right].$$

The terms $(\boldsymbol{\nabla}\cdot(\overline{\mathbf{u}'\zeta'}) + \overline{w'(\partial\zeta'/\partial z)})\,\partial\bar{\sigma}/\partial z$ represent the horizontal and vertical advection of relative vorticity by transient eddy fluxes. The terms $\bar{Q}\overline{(\mathbf{u}'\cdot\boldsymbol{\nabla})\sigma'}(\partial\bar{\sigma}/\partial z)^{-1} + \bar{Q}\,\overline{w'\partial\sigma'/\partial z}(\partial\bar{\sigma}/\partial z)^{-1}$ show the influence of transient eddy fluxes of tracer on the overall PV budget. The term $(f + \zeta)(\partial\bar{\mathbf{u}}/\partial z\cdot\boldsymbol{\nabla})\bar{\sigma}$ would be zero if $\partial\bar{\mathbf{u}}/\partial z$ were precisely proportional to $\mathbf{k}\times\boldsymbol{\nabla}\sigma$; the residual effects of this term occur mainly because σ represents potential density rather than in situ pressure, which should be used to correctly calculate geostrophic velocities. Finally $A_m\nabla^4\zeta\partial\bar{\sigma}/\partial z$ is the horizontal diffusion of relative vorticity, and

$$\bar{Q}\frac{\partial}{\partial z}\left[A_h\nabla^4\bar{\sigma}\left(\frac{\partial\bar{\sigma}}{\partial z}\right)^{-1}\right]$$

is the influence of the horizontal diffusion of density on the total vorticity budget. In addition to these terms, the PV analysis also includes error terms stemming from estimating the continuous derivatives required for PV balances from a discretized numerical model; however, they are not the dominant terms controlling the PV balance as will be shown in the discussion that follows.

In Fig. 3 Q for the mean Semtner–Chervin model output on the $\sigma_1 = 32.3$ surface is shown. It varies by about a factor of 2 across the Southern Ocean, with a substantial meridional gradient across the core of the ACC at the southern limit of the contoured values. The inhomogeneities in Q in turn suggest that inhomogeneous forcing is stronger than background eddy diffusion so that PV is not homogenized on this isopycnal.

b. Is potential vorticity conserved on streamlines?

Although diffusion is insufficient to homogenize Q, we might nonetheless predict that PV could be nearly conserved along streamlines. Consider the steady-state case, so that the tendency terms are zero. If PV values on streamlines are reset at one location along their circumpolar path, perhaps due to a localized topographic

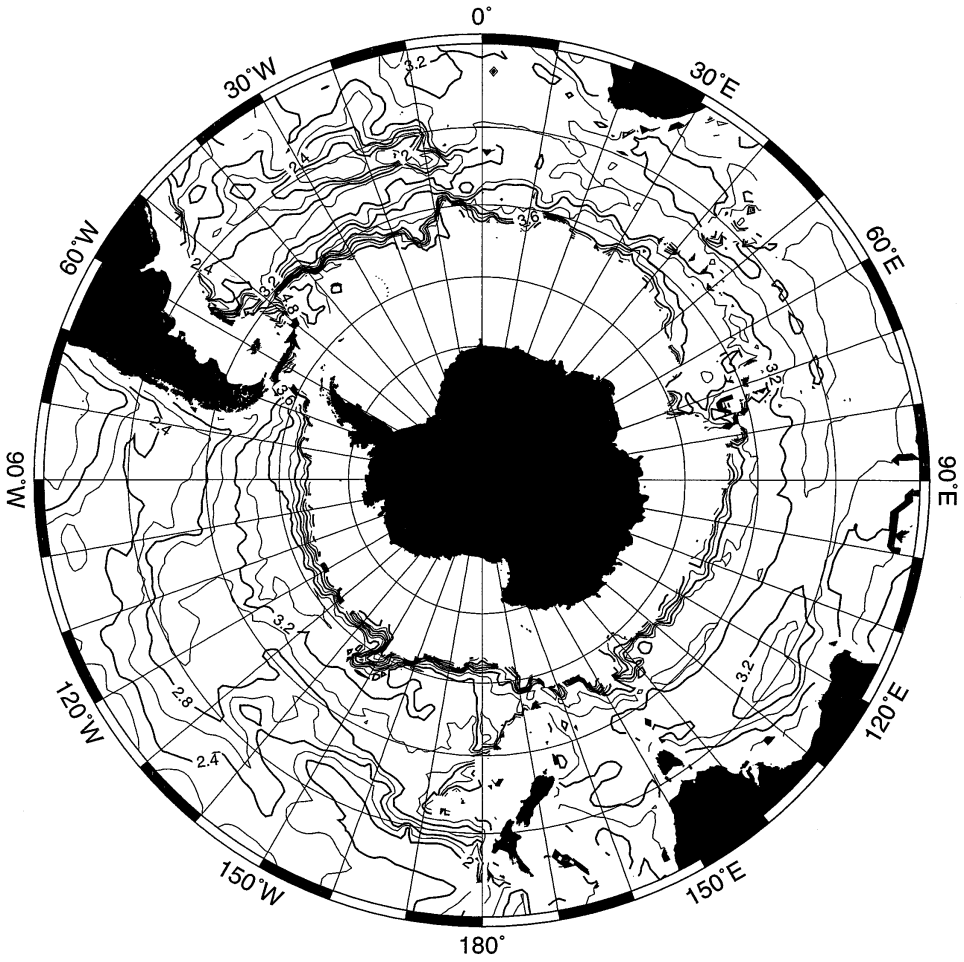

FIG. 3. PV, $(f + \zeta)\partial\sigma/\partial z$, (in kg s^{-1} m^{-4} $\times$ 10^8) on the σ_1 surface 32.3 determined from mean quarter-degree Semtner–Chervin model output. The σ_1 surface outcrops at the southern limit of the domain and is several kilometers deep at the northern limit. Points where $\sigma_1 = 32.3$ is shallower than 500 m have been eliminated.

forcing, then we predict that background diffusion and eddy processes will not be able to homogenize PV on the isopycnal surface. Under these conditions, assuming no diapycnic effects and no ageostrophic velocity, Q should be constant along streamlines. In this case, (9) would reduce to $J(\bar{M}, \bar{Q}) + f\bar{w}\partial\bar{Q}/\partial z = 0$, and Q would be exactly conserved along the depth-varying time-mean streamlines defined by $\bar{M}$.

In order to examine to what extent PV is conserved on streamlines, PV is computed along contours of constant Montgomery streamfunction on the potential density surface $\sigma_1 = 32.3$ in the Semtner–Chervin model output. Figure 4a shows that PV varies by about 25% along two representative streamlines, increasing steadily across the Pacific between 180° and 60°W and dropping sharply just downstream of Drake Passage around 40°W. PV variations across the Atlantic and Indian Oceans are more gradual, but indicate noteworthy rapid fluctuations near Kerguelen Island at 60°E and in the eddy-active region near the Macquarie Ridge and Campbell Plateau from 150°E to 180°.

In contrast with the gradual changes in PV along streamlines in Fig. 4a, PV undergoes dramatic fluctuations along lines of constant latitude, particularly where the isopycnal rises into the thermocline at the southern limit of the region and at Drake Passage (60°W), as shown in Fig. 5. Thus, in comparison with its large zonal variations, PV is nearly conserved along streamlines. The variations that occur are indications that even on this subsurface streamline, the curl of the net forces driving the mean ocean is nonzero. The remainder of this subsection will examine how PV changes qualitatively in response to this forcing.

Figures 4b–d show the relative importance of each of the components of PV. The major variations are attributed to changes in the layer thickness ($\partial z/\partial\sigma$), while variations in latitude (f) have less significant effects and relative vorticity is negligible. That PV variations along

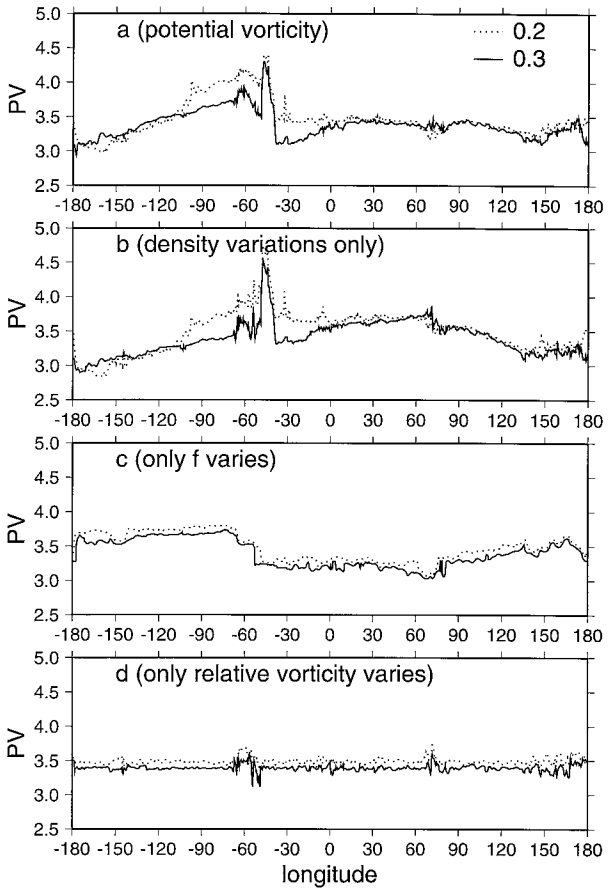

FIG. 4. (a) PV (in kg s^{-1} m^{-4} $\times$ 10^8) along two Montgomery streamfunction contours, *M*, from the Semtner–Chervin quarter-degree mean model output. Contours used correspond to 0.2 and 0.3 m (which have mean depths of 970 and 1170 m, thus bracketing the 1000-m reference depth.) Sea surface height increases toward the equator, so that the 0.3-m contour is north of the 0.2-m contour. (b) PV along Montgomery streamfunction, when $f + \zeta$ is fixed so that only changes in the stratification $\partial\sigma/\partial z$ are assessed. (c) PV along Montgomery streamfunction, where stratification and relative vorticity are held constant, so that only changes in latitude are assessed. (d) PV along Montgomery streamfunction, when f and $\partial\sigma/\partial z$ are held fixed so that only the effect of relative vorticity is considered.

streamlines are dominated by stratification changes rather than Coriolis parameter changes has clear implications for simple PV models of the ACC. Although Killworth (1992) noted that the vertical structure of the Southern Ocean may easily be represented using a self-similar profile, the dominant changes in PV, even at middepth, appear as changes in the vertical density profile. Thus, simple models that take advantage of this self-similar structure (e.g., Gille 1995; Marshall 1995; Krupitsky et al. 1996) are unlikely to represent the leading processes governing changes in PV.

In the vertically integrated vorticity balance analyzed by Wells and de Cuevas (1995), basic Sverdrup dynamics apply: wind stress curl is balanced by the barotropic meridional velocity multiplied by β (that is, $\mathbf{U}\cdot\nabla f \approx$ curl τ/ρ_o), and in the Drake Passage region, bottom pressure torque removes vorticity input by the wind. In contrast, on this isopycnal surface, stratification changes along streamlines provide the major compensation for the forcing.

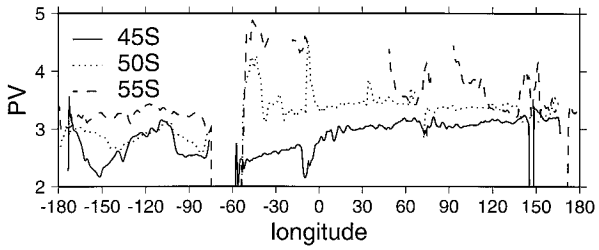

FIG. 5. PV (in kg s^{-1} m^{-4} $\times$ 10^8) along latitude lines, computed from Semtner–Chervin model output. Latitude lines shown correspond to 45°S, 50°S, and 55°S.

If we integrate (9) vertically, we predict that a Sverdrup-like balance should hold: $\int_{-H}^{0}(\partial\sigma/\partial z)^{-1}\mathbf{u}\cdot\nabla(f\partial\sigma/\partial z)dz$ = curl τ/ρ, where the wind stress τ is introduced in the surface boundary conditions. Examining the sign of the PV (here $f\partial\sigma/\partial z$) in comparison with the sign of the wind stress curl helps explain the numerical results. The ECMWF wind stress curl is positive to the north of about 50°S. The stratification term $\partial\sigma/\partial z$ is negative, while **u** in the direction of the streamline is positive by definition. Thus, in the Atlantic and Indian sectors of the Southern Ocean, where the ACC is north of 50°S, PV tends to decrease along streamlines. Where the ACC is farther south and wind stress curl is negative, PV tends to increase.

The middepth surface $\sigma_1 = 32.3$ is between 1500 and 500 m deep along the 0.2-m and 0.3-m streamlines, as shown in Fig. 6. Thus, the isopycnal layer is far below the ocean's surface and is not directly wind forced; surface wind forcing is conveyed indirectly to the middepth layers of the ocean model. Figure 6b indicates that the layer thickness decreases as the layer shoals so that PV

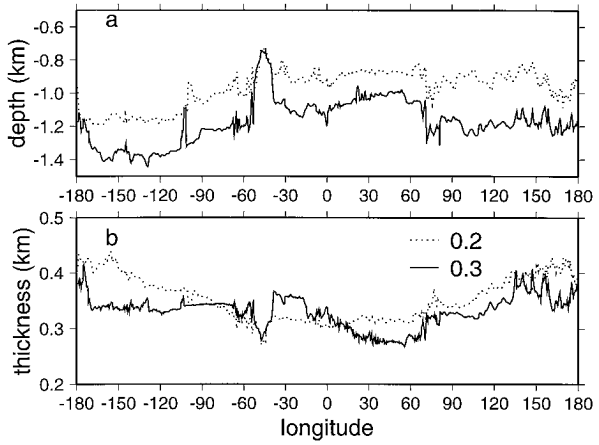

FIG. 6. (a) Depth of the $\sigma_1 = 32.3$ isopycnal surface in kilometers along streamlines. (b) Thickness of the isopycnal layer corresponding to $32.25 < \sigma_1 < 32.35$, in km.

is larger where the isopycnal surface is shallower. This is consistent with a simple concept of the wind-driven flow in the Southern Ocean. Since the stratification and alongstream velocity are of constant sign, the alongstream derivative of PV, $\partial Q/\partial s$, should be proportional to the curl of the wind stress. In addition, wind stress curl should induce an Ekman pumping vertical velocity, so that $\text{curl}(\tau) \propto -fw_{\text{Ek}}$, where w_{Ek} is the vertical velocity at the base of the Ekman layer. The vertical velocity w throughout the water column is assumed to be roughly w_{Ek} and may be written as $w = u_s \partial d/\partial s$, where d is the depth of an isopycnal. The terms u_s and f are of constant sign and slowly varying. This leads to $\text{curl}(\tau) \propto \partial Q/\partial s \propto \partial d/\partial s$. This relation therefore suggests that the depth of the isopycnal should vary with Q and, since Q variations are dominated by changes in stratification (or the reciprocal of layer thickness), stratification should increase (and correspondingly layer thickness decrease) roughly in locations where the wind stress curl brings isopycnals toward the surface, as the model results in Fig. 6 indicate.

c. Forcing terms on streamlines

The behavior of middepth PV in response to wind forcing can only be interpreted in generalities using Figs. 4 and 6. To better understand what controls the variations in PV, compare the value of PV with the forcing terms controlling it. Each of the terms in (9) is projected into stream coordinates (s, c), where s is the alongstream direction and c is the cross-stream direction. Expanding the Jacobian operator and vertical advection terms from the left-hand side of (9) produces

$$\frac{1}{f} J(\bar{M}, \bar{Q}) + (\bar{\mathbf{u}}\cdot\boldsymbol{\nabla})\bar{\sigma}\frac{\partial \bar{Q}}{\partial z}\left(\frac{\partial \bar{\sigma}}{\partial z}\right)^{-1} = u_s \frac{\partial Q}{\partial s}, \quad (11)$$

where u_s is the alongstream, along-isopycnal velocity, and the cross-stream velocity u_c is 0 by definition.

The change in PV of a particle traveling a distance s along a streamline is found by substituting (11) into (9) and integrating, so that

$$\begin{aligned}
\bar{Q}(s) - \bar{Q}(0) = &- \int_0^s \frac{\zeta_f - \zeta_i}{u_s \Delta t}\frac{\partial \bar{\sigma}}{\partial z}\, ds' - \int_0^s \frac{\bar{Q}}{u_s}\frac{\partial}{\partial z}\left[\frac{\sigma_f - \sigma_i}{\Delta t}\left(\frac{\partial \bar{\sigma}}{\partial z}\right)^{-1}\right] ds' - \int_0^s \left(\boldsymbol{\nabla}\cdot\overline{(\mathbf{u}'\zeta')} + \overline{w'\frac{\partial \zeta'}{\partial z}}\right)\frac{\partial \bar{\sigma}}{\partial z}\frac{1}{u_s}\, ds' \\
&- \int_0^s \frac{\bar{Q}}{u_s}\overline{(\mathbf{u}'\cdot\boldsymbol{\nabla})\sigma'}\left(\frac{\partial \bar{\sigma}}{\partial z}\right)^{-1} ds' - \int_0^s \frac{\bar{Q}}{u_s}\overline{w'\frac{\partial \sigma'}{\partial z}}\left(\frac{\partial \bar{\sigma}}{\partial z}\right)^{-1} ds' - \int_0^s \frac{(f + \bar{\zeta})}{u_s}\left(\frac{\partial \bar{\mathbf{u}}}{\partial z}\cdot\boldsymbol{\nabla}\right)\bar{\sigma}\, ds' \\
&+ \int_0^s \frac{A_m}{u_s}\nabla^4\bar{\zeta}\frac{\partial \bar{\sigma}}{\partial z}\, ds' + \int_0^s \frac{\bar{Q}}{u_s}\frac{\partial}{\partial z}\left[A_h\nabla^4\bar{\sigma}\left(\frac{\partial \bar{\sigma}}{\partial z}\right)^{-1}\right] ds'. \quad (12)
\end{aligned}$$

The terms in (12) represent the alongstream integrals of each of the terms in (9). Thus (12) shows that the alongstream integrated form of any term in the PV equation divided by alongstream velocity will represent the PV variations due to that term.

Figure 7a shows a comparison of $\bar{Q}$ computed locally at each point along a streamline (solid line) and $\bar{Q}$ determined by integrating along a streamline, following the method defined in (12). Although integrating numerical model output along streamlines may seem like an unreliable computation, the results in Fig. 7a indicate that both small-scale and large-scale variations are successfully recovered in the calculation. Tests have shown that the discrepancies between the two lines in Fig. 7a are not due to ageostrophic effects, which are considerably smaller in magnitude. Instead the differences can be attributed to integration errors incurred in locations where $\bar{Q}$ changes value sharply (e.g., 95°W, 30°W). In these spots, the combination of interpolation and integration is not able to capture the local variations in $\bar{Q}$ precisely, and small offsets are introduced into the integrated $\bar{Q}$ estimate. The isolated sources and small magnitude of the error suggests that integration problems will not significantly influence the results. The vorticity balance in (12) does close, and this presentation allows us to consider which terms in the PV balance are actually responsible for the changes in $\bar{Q}$ along streamlines.

Figure 7b indicates that the PV balance is significantly affected by the transient eddy processes due to tracer advection, transient eddy processes due to momentum advection, the tracer tendency, horizontal momentum diffusion, and horizontal tracer diffusion. The transient tracer flux and transient momentum flux terms (identified as tracer advection and momentum advection in the figure caption) are calculated as residuals from the tracer and momentum balances, respectively, since the model archiving scheme does not include sufficient detail to recover the transient component of the PV balance. The importance of the transient tracer and momentum advection terms suggests that a balance that neglected these terms would lack essential portions of the physics [as Killworth and Nanneh (1994) also noted for the isopycnic momentum and volume budgets]. The

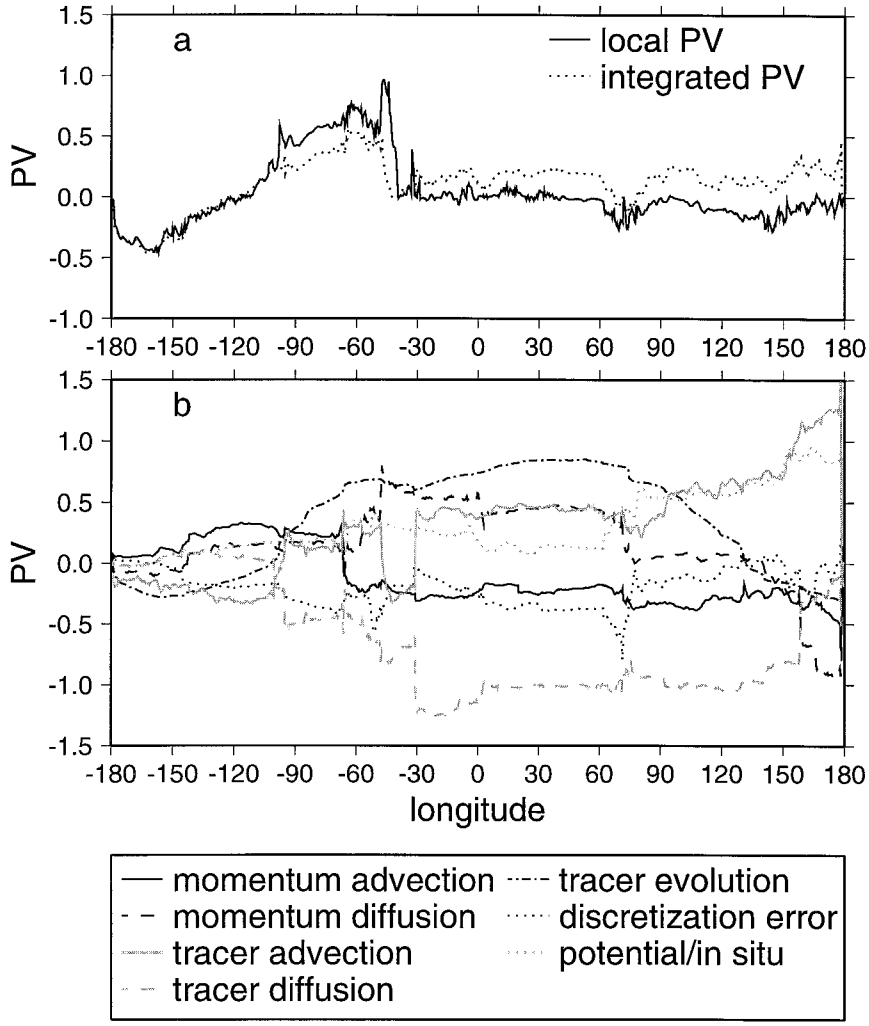

FIG. 7. (a) PV (in kg s^{-1} m^{-4} $\times$ 10^8) along the 0.2-m Montgomery streamfunction (solid line) compared with PV estimated by integrating the quantity $[J(\overline{M}, \overline{Q}) + (\overline{\mathbf{u}}\cdot\boldsymbol{\nabla})\overline{\sigma}\partial\overline{Q}/\partial z(\partial\overline{\sigma}/\partial z)^{-1}]/(fu_s)$ along the same streamline. (b) Forcing terms responsible for changes in PV along the 0.2-m streamline. The momentum advection and tracer advection terms refer to transient eddy fluxes, while the potential/in situ term results from potential and in situ density surfaces not coinciding, so that $[(\partial\overline{\mathbf{u}}/\partial z)\cdot\boldsymbol{\nabla}]\overline{\sigma}$ is not zero. All terms are set to 0 at 180°W. Together tracer advection, tracer evolution, and momentum advection capture the leading variations in PV, while momentum and tracer diffusion play significant but smaller roles.

results found for this 0.2-m streamline closely resemble those on adjacent streamlines: No single process appears to explain the entire PV balance in Fig. 7b. However, note that many of the small-scale variations ($<10°$ longitude) in PV in Fig. 7a are explained by the tracer advection term, while the large-scale trends ($>50°$) are partially captured by the sum of the tracer evolution, transient tracer advection, and transient momentum advection terms. In addition the large-scale momentum and tracer diffusion variations often balance each other, so that the net influence of diffusion may be less than the apparent influence in either the momentum or tracer equations. The term designating the PV changes induced because isopycnic and in situ density surfaces are not coincident also influences the PV balance; in essence, this term is a measure of the error inherent in investigating PV along isopycnals. Finally, the discretization error is uniformly small. In addition to the terms plotted in Fig. 7b, recall that the vertical viscosity term, relative vorticity tendency, ageostrophic advection, and diapycnal flux terms were judged to have no significant impact on the PV balance and are not shown.

Because the tracer tendency term plays a significant role in the overall alongstream PV balance, these results suggest that the Semtner–Chervin model may not have spun up sufficiently, so the middepth isopycnals did not reach steady state. If the model reached a quasi-stationary state it might have a different PV balance. How-

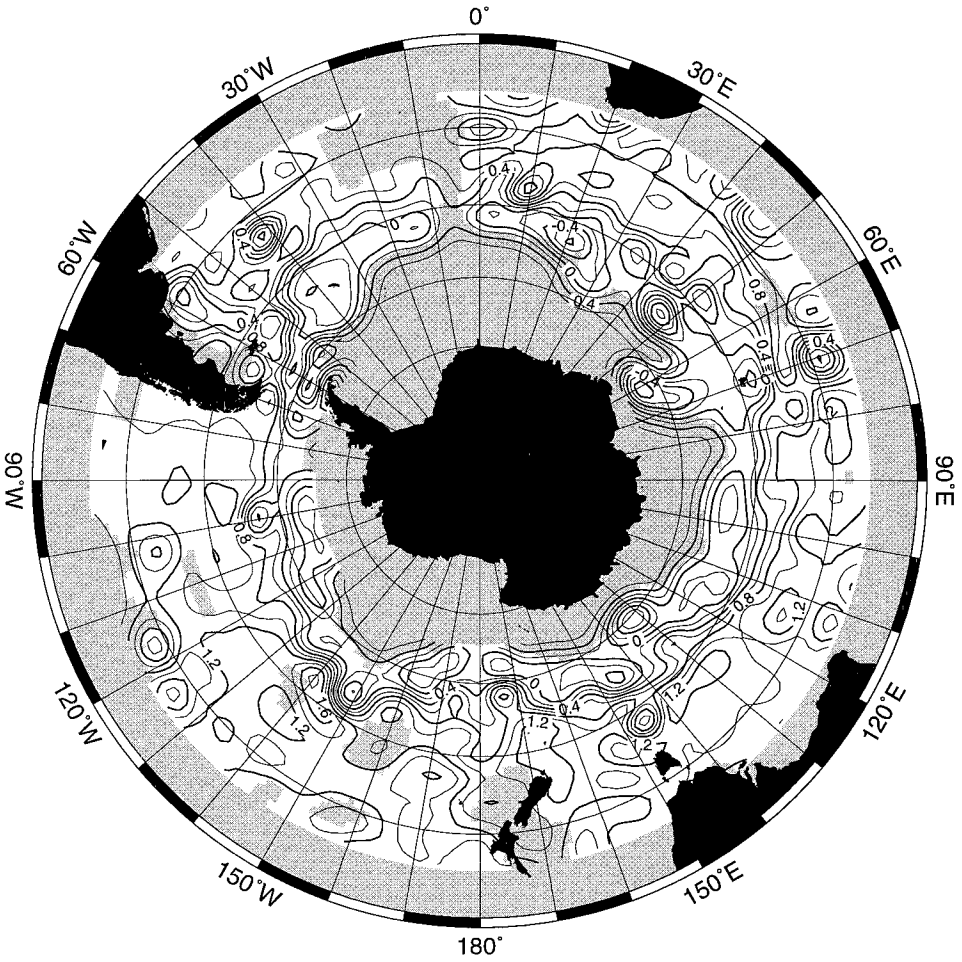

FIG. 8. Montgomery streamfunction M [as defined in (2) in m × 0.1] on the isopycnal surface $\sigma_1 = 32.3$ referenced to the isopycnal surface $\sigma_1 = 32.4$. The contour interval is 0.02 m, and the total range is small because of the relatively shallow reference layer but should nonetheless be representative of physical processes. Gray areas indicate regions with no mapped data and regions where the formal error from the objective mapping procedure exceeds 80% of the overall data variance, which is about 0.006 m.

ever, to the extent that the numerical ocean does resemble the real ocean, this analysis suggests that transient eddy effects play a substantial role in the PV balance along mean streamlines. In particular, transient tracer fluxes appear directly responsible for small-scale PV variations along streamlines. Since transient tracer processes are often associated with the vertical transfer of momentum input by the wind via interfacial form drag (Johnson and Bryden 1989; Marshall et al. 1993), this might be an indication that indirect wind forcing is one of the factors responsible for changes in PV along mean streamlines at middepth in the ACC.

3. Potential vorticity from Southern Ocean hydrography

For comparison with the numerical results, PV may also be calculated using hydrographic data compiled by Olbers et al. (1992, hereafter OGSS). OGSS produced objectively mapped data fields with 1° resolution at 38 depth levels; however, for this study their compiled hydrographic data were used so that all mapping could be done along isopycnal surfaces. This was done specifically to avoid the types of averaging problems discussed by Lozier et al. (1994) who pointed out that smoothing quantities along level surfaces and then mapping them onto isopycnals would produce substantially different results than would smoothing the data along isopycnal surfaces. [Nonetheless, the results in this section would not be changed qualitatively if PV and streamlines were instead computed directly from the gridded quantities produced by OGSS (Gille 1995).] At each hydrographic station, PV and the Montgomery streamfunction were computed on the isopycnal surface $\sigma_1 = 32.3$. Since PV varies in the upper ocean due to mixed layer processes, data points were retained only if they were deeper than 500 m; as a result, data points at the southern limit of the domain were eliminated. Following the general

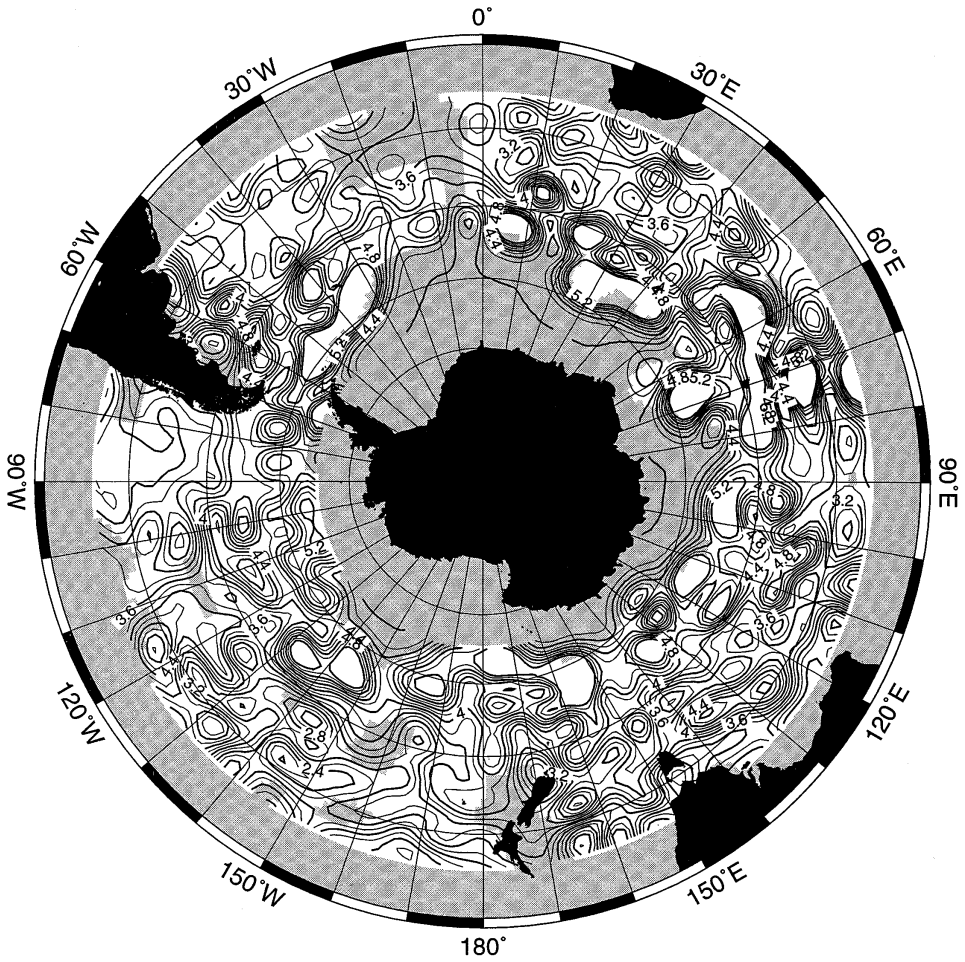

FIG. 9. PV, $f\partial\sigma/\partial z$ (in kg s^{-1} m^{-4} $\times$ 10^{8}), on the σ_1 surface 32.3 determined from hydrographic data. Gray areas indicate regions with no mapped data and regions where the formal error from the objective mapping procedure exceeds 80% of the data variance, which is 1×10^{8} for the entire domain.

methodology outlined by OGSS, for both PV and Montgomery streamfunction, outliers were removed if they differed from the mean by more than three standard deviations. To reduce errors associated with the erroneous values initially in the dataset, the outlier test was repeated. The resulting dataset consisted of 2571 points scattered throughout the Southern Ocean, but concentrated primarily in the South Atlantic. Unlike the numerical model output, which includes a known sea surface topography, for the hydrographic data a reference surface must be assigned. The Montgomery streamfunction was referenced to the slightly deeper isopycnal surface, $\sigma_1 = 32.4$; this shallow reference density was selected because using a denser reference layer would result in extensive data dropout wherever the deeper isopycnal surface intersects the ocean bottom. Therefore, instead of imagining the velocity to be zero on the reference layer, consider it to attenuate smoothly below this depth.

The resulting data were objectively mapped using a Gaussian correlation function, with a 450-km decorrelation length in the zonal direction and 350 km in the meridional direction, as done by OGSS. Gille (1994) noted that these length scales are almost double what the mean fields reconstructed from altimeter data indicate, and they may therefore result in fields smoother than the oceanic mean fields. Extensive smoothing should help to minimize problems associated with nonsynopticity of the data and sparse sampling in the Southern Ocean.

Figure 8 shows the mapped Montgomery streamfunction on the isopycnal surface $\sigma_1 = 32.3$. PV on the $\sigma_1 = 32.3$ surface from the hydrographic data is shown in Fig. 9. Despite the expectation that the objectively mapped fields should be smooth renditions of the hydrographic measurements, the objectively mapped PV shows substantial variability over relatively short length scales, in contrast with the numerical model PV (Fig. 3). This may indicate that the historic hydrographic record is not extensive enough to represent accurately the climatological mean state of the Southern Ocean, but it could also indicate that the dominant length scales in

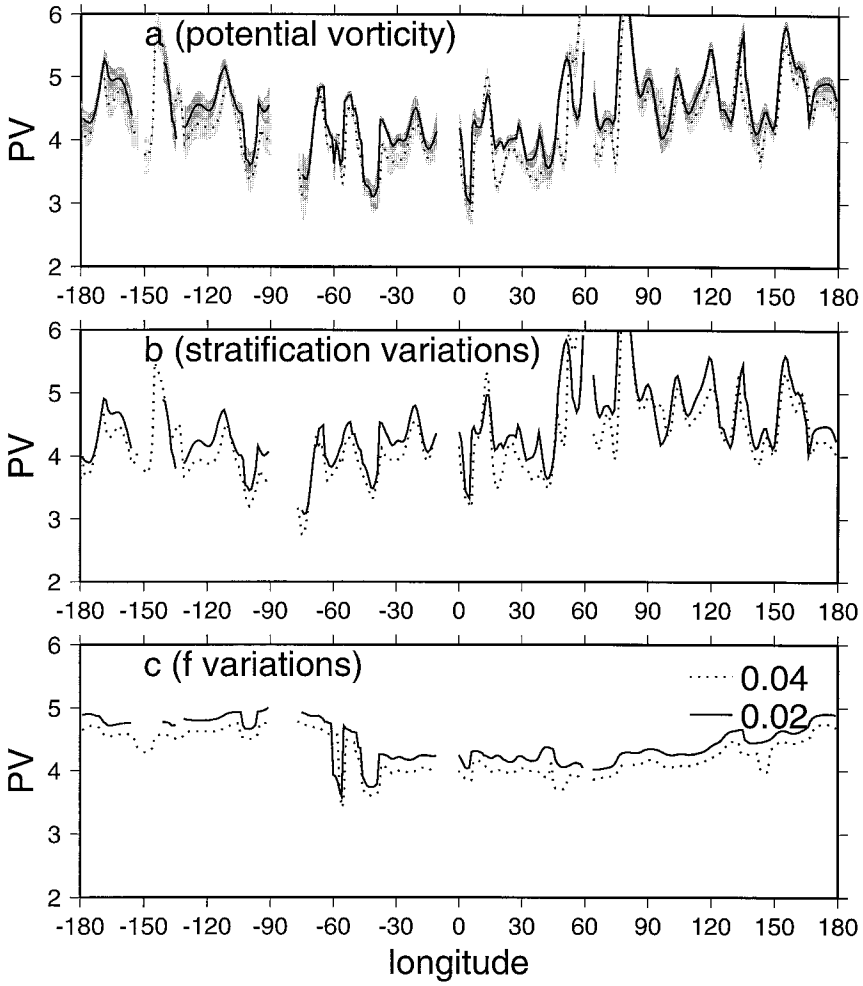

FIG. 10. (a) PV (in kg s^{-1} m^{-4} $\times$ 10^8) along Montgomery streamlines determined from the OGSS atlas data. Height contours correspond to the contours labeled 0.04 and 0.02 in Fig. 8. Gray regions indicate the one standard deviation formal error bars from objective mapping. (b) PV along Montgomery streamlines when f is held fixed so that only changes in stratification are assessed. (c) PV along Montgomery streamlines when $\partial z/\partial\sigma$ is held fixed so that only the effects of changing latitude are assessed.

the numerical model output are longer than in the real ocean. Because PV is computed on isopycnals directly from hydrographic data and then objectively mapped, rather than being determined from the objectively mapped fields, the results shown in Fig. 9 appear different than PV maps produced by Marshall et al. (1993). However, like the numerical model PV (Fig. 3), the PV shown in Fig. 9 is consistent with that plotted by Marshall et al. and by You and McDougall (1990) in showing that PV may change by a factor of 2 or more in the circumpolar portion of the Southern Ocean.

Potential vorticity variations along Montgomery streamlines (shown in Fig. 10) are comparable in magnitude to the variations seen in numerical model output, but the variations occur over much shorter distances and could represent rather different physical processes. As in the numerical model results in Fig. 4, alongstream changes in PV are predominantly due to stratification changes rather than Coriolis parameter changes as indicated by the large fluctuations in Fig. 10b compared with Fig. 10c.

If the atlas data are representative of Southern Ocean stratification, then the results indicate that the ACC undergoes substantial changes in PV over relatively short distances. The high wavenumber variations in PV on streamlines could be an indication that PV is input by the wind at higher wavenumbers than ECMWF winds would suggest or that it is dissipated due to bottom pressure torques associated with midsized topographic features that the model does not seem to feel, as Gille's (1997) momentum balance analysis suggests. Thus, the differences between Figs. 4 and 10 might be explained by identifiable differences between the model and the real ocean.

Alternatively, rather than thinking about model−ocean differences, note also that nonsynopticity and smoothing make the atlas data a suboptimal proxy for PV and streamfunctions, so the differences between Figs. 4 and 10 may simply be a result of the sparseness of the hydrographic record. The transient eddy processes shown in the model results are not distinguished by the data sampling, and in the limited available hydrographic record, temporal variability may be aliased to appear as a spatially varying mean field. Thus, readers who are uncomfortable interpreting the hydrographic data as indicating high-wavenumber variations in PV may prefer to conclude that the limited hydrographic measurements south of 30°S resemble instantaneous snapshots of an eddy rich field, and the sampling has not been sufficiently frequent to resolve the mean structure of the Southern Ocean.

4. Discussion and summary

The results of this investigation have several implications for Southern Ocean studies.

First, within statistical error bars PV does not appear to be uniform, neither in the Semtner–Chervin model output nor in hydrographic data. PV differs by 50% over 1000-km length scales and has a substantial mean gradient across the width of the ACC. These results suggest that forcing and dissipation of PV at middepth in the ACC are too irregular to result in uniformly homogenized PV.

Second, in addition to being inhomogeneous on isopycnal surfaces, middepth PV is also not conserved along mean streamlines on isopycnal surfaces, suggesting that some apparent forcing drives PV and that the influence of this forcing is not dissipated precisely in the locations where it enters. In both numerical model output and hydrographic data, changes in PV are largely due to stratification changes rather than changes in planetary vorticity along streamlines. Stratification changes are not precisely related to the locations of bathymetry, so are not easily represented as a simple topographic torque due to sea floor topography. Thus, simple self-similar models of the ACC that assume uniform stratification and predictable responses to bathymetry may not adequately capture dominant PV variations along the path of the ACC.

Third, variations in PV are qualitatively consistent with a simple notion that the middepth system responds in part to changes in wind stress curl. In a detailed analysis of the numerical model PV balance, no single factor emerges as the dominant mechanism responsible for PV changes along streamlines. Thus, to answer the question implicit in this paper's title, potential vorticity is not conserved along mean streamlines in the Semtner–Chervin Southern Ocean, because a half dozen terms in the PV equation all conspire to keep it from being conserved. Significant contributions to the PV balance come from transient tracer fluxes, the tracer tendency term, transient momentum fluxes, tracer diffusion, momentum diffusion, and a term associated with the isopycnal surface not being identical to a constant in situ density surface. The transient tracer flux contribution captures many of the high-wavenumber PV variations; since this term is sometimes associated with the vertical flux of wind stress via interfacial form drag, its apparent importance may be an indicator that the middepth ACC does feel surface wind forcing, at least indirectly, but that this process only accounts for a portion of the alongstream PV balance.

Acknowledgments. Many thanks to Bert Semtner and Bob Chervin who made their model results readily available and to Tony Craig and Robin Tokmakian who helped in extracting and interpreting the data. This study benefited from discussions with Kathie Kelly, Mike McCartney, John Marshall, John Toole, Terry Joyce, and Russ Davis. Trevor McDougall and several anonymous reviewers made invaluable suggestions, which have helped to shape the analysis and presentation. Joe LaCasce, Stefan Llewellyn Smith, and Lynne Talley also provided useful comments on an earlier version of the manuscript. This work was supported by National Aeronautics and Space Administration Contract NAGW-1666 and by National Oceanic and Atmospheric Administration Award NA47GP0188 to the Lamont/Scripps Consortium for Climate Research.

REFERENCES

Andrews, D. G., J. R. Holton, and C. B. Leovy, 1987: *Middle Atmosphere Dynamics.* Academic Press, 489 pp.

FRAM Group, 1991: An eddy-resolving model of the Southern Ocean. *Eos, Trans. Amer. Geophys. Union,* **72,** 169–175.

Gille, S. T., 1994: Mean sea surface height of the Antarctic Circumpolar Current from Geosat data: Method and application. *J. Geophys. Res.,* **99,** 18 255–18 273.

——, 1995: Dynamics of the Antarctic Circumpolar Current: Evidence for topographic effects from altimeter data and numerical model output. Ph.D. dissertation, Massachusetts Institute of Technology/Woods Hole Oceanographic Institution Joint Program, 216 pp. [Available from Document Library, Woods Hole Oceanographic Institution, Woods Hole, MA 02543.]

——, 1997: The Southern Ocean momentum balance: Evidence for topographic effects from numerical model output and altimeter data. *J. Phys. Oceanogr.,* in press.

Hellerman, S., and M. Rosenstein, 1983: Normal monthly wind stress over the world ocean with error estimates. *J. Phys. Oceangr.,* **13,** 1093–1104.

Ivchenko, V. O., K. J. Richards, and D. P. Stevens, 1996: The dynamics of the Antarctic Circumpolar Current. *J. Phys. Oceanogr.,* **26,** 753–774.

Johnson, G. C., and H. L. Bryden, 1989: On the size of the Antarctic Circumpolar Current. *Deep-Sea Res.,* **36,** 39–53.

Killworth, P. D., 1992: An equivalent-barotropic mode in the Fine Resolution Antarctic Model. *J. Phys. Oceanogr.,* **22,** 1379–1387.

——, and M. M. Nanneh, 1994: Isopycnal momentum budget of the Antarctic Circumpolar Current in the Fine Resolution Antarctic Model. *J. Phys. Oceanogr.,* **24,** 1201–1223.

——, D. Stainforth, D. J. Webb, and S. M. Paterson, 1991: The development of a free-surface Bryan–Cox–Semtner ocean model. *J. Phys. Oceanogr.,* **21,** 1331–1348.

Krupitsky, A., V. M. Kamenkovich, N. Naik, and M. A. Cane, 1996:

A linear equivalent barotropic model of the Antarctic Circumpolar Current with realistic coastlines and bottom topography. *J. Phys. Oceanogr.*, **26,** 1803–1824.

Levitus, S., 1982: *Climatological Atlas of the World Ocean.* NOAA Prof. Paper No. 13, U.S. Govt. Printing Office, Washington, DC, 173 pp.

Lozier, M. S., M. S. McCartney, and W. B. Owens, 1994: Anomalous anomalies in averaged hydrographic data. *J. Phys. Oceanogr.*, **24,** 2624–2638.

Marshall, D., 1995: Topographic steering of the Antarctic Circumpolar Current. *J. Phys. Oceanogr.*, **25,** 1636–1650.

Marshall, J., D. Olbers, H. Ross, and D. Wolf-Gladrow, 1993: Potential vorticity constraints on the dynamics and hydrography of the Southern Ocean. *J. Phys. Oceanogr.*, **23,** 465–487.

McDougall, T. J., 1989: Streamfunctions for the lateral velocity vector in a compressible ocean. *J. Mar. Res.*, **47,** 267–284.

Müller, P., 1995: Ertel's potential vorticity theorem in physical oceanography. *Rev. Geophys.*, **33,** 67–97.

Olbers, D., V. Gouretski, G. Seiß, and J. Schröter, 1992: *Hydrographic Atlas of the Southern Ocean.* Alfred Wegener Institute, 18 pp. and 82 plates.

Pedlosky, J., 1987: *Geophysical Fluid Dynamics.* 2d ed. Springer-Verlag, 710 pp.

Rhines, P. B., and W. R. Young, 1982: Homogenization of potential vorticity in planetary gyres. *J. Fluid Mech.*, **122,** 347–367.

Semtner, A. J., 1986: Finite-difference formulation of a world ocean model. *Proceedings of the NATO Study Institute on Advanced Physical Oceanographic Numerical Modelling*, J. J. O'Brien, Ed., Reidel, 187–202.

——, and R. M. Chervin, 1992: Ocean general circulation from a global eddy-resolving model. *J. Geophys. Res.*, **97,** 5493–5550.

Stevens, D. P., and V. O. Ivchenko, 1997: The zonal momentum balance in a realistic eddy resolving general circulation model of the Southern Ocean. *Quart. J. Roy. Meteor. Soc.*, in press.

Trenberth, K. E., J. G. Olson, and W. G. Large, 1989: A global ocean wind stress climatology based on ECMWF analyses. Tech. Rep. NCAR/TN-338+STR, 93 pp. [Available from National Center for Atmospheric Research, Boulder, CO 80307-3000.]

Wells, N. C., and B. A. de Cuevas, 1995: Depth-integrated vorticity budget of the Southern Ocean from a general circulation model. *J. Phys. Oceanogr.*, **25,** 2569–2582.

You, Y., and T. J. McDougall, 1990: Neutral surfaces and potential vorticity in the world's oceans. *J. Geophys. Res.*, **95,** 13 235–13 261.

Zhang, H.-M., and N. G. Hogg, 1992: Circulation and water mass balance in the Brazil Basin. *J. Mar. Res.*, **50,** 385–420.